The following publication Q. Wang, S. Niu and L. Yang, "Design Optimization and Comparative Study of Novel Dual-PM Excited Machines," in IEEE Transactions on Industrial Electronics, vol. 64, no. 12, pp. 9924-9933, Dec. 2017 is available at https://doi.org/10.1109/TIE.2017.2716869

Design Optimization and Comparative study of Novel Dual-PM Excited Machines

Qingsong Wang, Shuangxia Niu, *Member, IEEE* and Lin Yang

***Abstract*—This paper systematically studies a new kind of PM machines with both stator and rotor PM excitations, namely, dual-PM excited machines. The key is to rely on the PM-iron structure in the machine to provide both PM excitation and flux modulation. Besides the fundamental field component in the air-gap, some other predominant harmonics introduced by the flux modulating effect can also contribute to the electromagnetic torque production. Therefore, this kind of machines can be designed with high torque density. Four dual-PM excited machine concepts with the same rotor configuration but different stator structures are comparatively studied, which include double-stator PM machine(DSPM), stator multi-tooth-PM machine(SMTPM), stator slot-PM machine(SSPM) and stator tooth-PM machine(STPM). Based on the flux modulating effect, the general design principle of the dual-PM machines is proposed in this paper. Through analytically investigating the air-gap field harmonics, the physical insight of the dual-PM machines is brought forward. All the four machines are optimized using an improved Tabu search coupled with finite element method (ITS-FEM), and their electromagnetic performances are comprehensively studied and compared. A prototype of STPM is manufactured. Experimental tests are conducted and the results well verify the electromagnetic design.**

***Index Terms*—Dual-PM machines, flux modulating, PM-iron structure, stator tooth-PM machine.**

I. INTRODUCTION

ELECTRIC machines play an important role in the modern industry. In addition, due to their theoretical zero emission, electric machines are especially popular in clean energy systems, such as electric vehicles and wind power generators, aiming to solve the problems of energy crisis and environmental pollution[1-7]. Among different types of electric machines, permanent magnet (PM) machines are recognized to be the most promising candidates with inherent high torque capability and high efficiency, and have been widely investigated by researchers.

Currently, PM machines are mostly employed with single-sided PMs, which include rotor-PM machines and stator-PM machines. The rotor-PM machines utilize the fundamental component of PM field and armature field to generate electromagnetic torque. The PMs can be either surface mounted on the rotor or inserted into the rotor, both of which are widely used in industrial applications. The main concerns of rotor-PM machines are the temperature rise at the PM region, since the rotor has poor heat dissipation, which may cause irreversible demagnetization of PMs [8]. When the PMs are surface mounted on the rotor, the PMs may be destroyed by the centrifugal force during high speeds [9]. Although additional retaining sleeves can be used to protect the PMs, the equivalent air-gap length is increased consequently [10]. Stator-PM machines can well solve the aforementioned problems. The PMs can be easily cooled when located on the stator, and the rotor only has salient poles, which is robust and suitable to be used in high-speed applications. Various stator-PM machines have been reported, including flux reversal PM machines [11-13], doubly salient PM machines [14-16] and flux switching PM machines [17-19]. The fundamental component of the magnetic field excited by the stator PMs is firstly modulated by the salient-pole rotor, then interacts with the armature field to produce electromagnetic torque.

To produce steady electromagnetic torque, the magnetic field excited by the PMs should interact with the armature field. The effective field components excited by the PMs should have the same pole-pair number (PPN) and the same rotational speeds with the armature field. In both rotor-PM machines and stator-PM machines, the fundamental component of PM field is used to produce steady electromagnetic torque, and other harmonics can only generate torque ripples.

This paper systematically studies a new class of PM machines with both stator and rotor PM excitations, namely, dual-PM excited machines. Besides the fundamental components excited by the PMs, some other predominant field harmonics introduced by the flux modulating effect can also contribute to the electromagnetic torque generation. Therefore, dual-PM excited machines can be designed with comparable or even higher torque capability than the single-sided PM machines. Moreover, as the PMs can be employed on the rotor and stator simultaneously, the PM arrangement in the dual-PM excited machines is more flexible, which can result in various machine configurations and rich the PM machine category. The general design principle of the dual-PM excited machines is analytically studied, and the field harmonics are analyzed in detail, which can provide an insight into the working principle

Manuscript received December 22, 2016; revised March 7, 2017, and May 2, 2017; accepted May 3, 2017. This work was supported by the Research Grant Council, Hong Kong Special Administrative Region, China, under projects PolyU 152130/14E and PolyU 15250916/16E. *(Corresponding author: Shuangxia Niu.)*

Qingsong Wang and Shuangxia Niu are with the Department of Electrical Engineering, The Hong Kong Polytechnic University, Hong Kong (e-mail: q.s.wang@connect.polyu.hk; eesxniu@polyu.edu.hk).

Lin Yang is with the State Power Economic Research Institute, Beijing, China(e-mail: eelinyang@163.com).

of the dual-PM excited machines. Four typical kinds of dual-PM excited machine configurations are presented and optimized using an improved Tabu search [20] coupled with finite element method (ITS-FEM), which include double-stator PM machine (DSPM), stator multi-tooth-PM machine (SMTPM), stator slot-PM machine (SSPM) and stator tooth-PM machine(STPM). Their electromagnetic performances are studied and quantitatively compared. The prototype of STPM is manufactured, and experimental tests are conducted to verify its electromagnetic design.

II. Typical Machine Configurations

The basis of the dual-PM excited machines relies on the PM-iron structure, in which the PMs and iron poles are separated with each other one by one, as shown in Fig. 1. All the PMs are magnetized in the same direction, that is radially outward/inward magnetized in rotating machines, or upward/downward in linear machines. Each PM and its adjacent iron pole forms a pair of magnetic poles. The PM-iron structure can provide both PM excitation and flux modulation, as the permeance difference between the PMs and the iron can change the reluctance distribution. Both inner rotor type and outer rotor type are appropriate designs. According to the stator configuration, the dual-PM machines can be typically categorized into four types, namely DSPM, SMTPM, SSPM and the STPM, as given in Fig. 2.

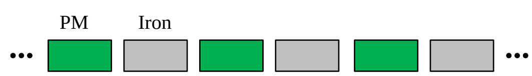

Fig. 1. Configuration of the PM-iron structure.

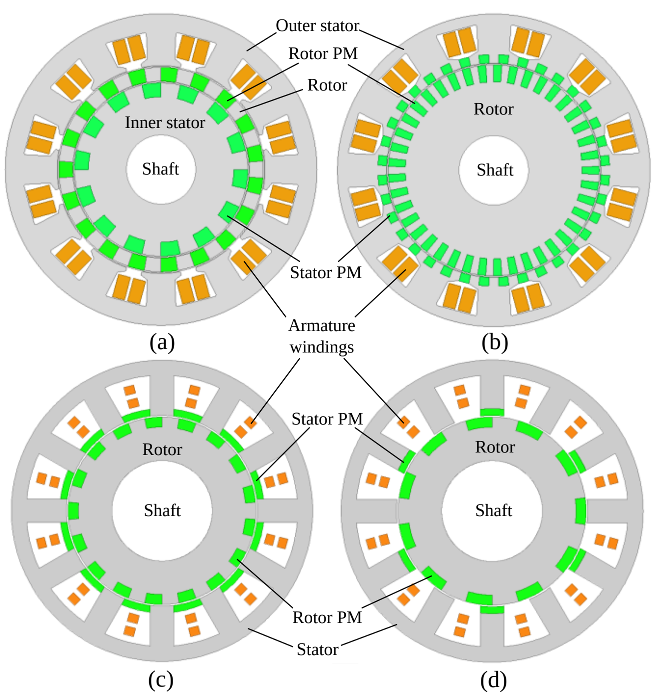

Fig. 2. Configurations of the dual-PM machines. (a) DSPM. (b) SMTPM. (c) SSPM. (d) STPM.

A. DSPM

The configuration of DSPM is given in Fig. 2(a), which consists of two stators and one rotor. The rotor is simply made up of PM-iron sequences, while the inner stator has an additional stator yoke and the armature windings are housed in the slots of outer stator. As there exists two air-gaps, the rotor should be designed as cup-shaped. The DSPM is developed from the triple-PM magnetic gear reported in [21], the outer rotor of the triple-PM magnetic gear is replaced by the outer stator in the DSPM.

B. SMTPM

Fig. 2(b) shows the configuration of SMTPM, each stator tooth has several sub-teeth. In fact, multi-tooth machines have already been investigated by researchers, as reported in [22, 23], but these machines have either no PM excitation or just single-sided stator-PM excitation. Multi-tooth dual-PM machine proposed in this paper can further enrich the machine category.

C. SSPM

Fig. 2(c) shows the configuration of the proposed SSPM, the stator PMs are employed on the slot openings. Each stator PM and its adjacent stator tooth will form a magnetic pole-pair, the stator tooth can also act as modulator to modulate the air-gap flux. Machines with PMs in the slot openings have been reported in [24], but only the stator have PM excitation, the rotor is made up of salient poles. SSPM with additional PM excitation in the rotor, as proposed in this paper, can achieve higher torque capability.

D. STPM

The configuration of the STPM is given in Fig. 2(d). The rotor structure of STPM is the same as that of the SMTPM and SSPM. The stator PMs are located on the surface of the stator teeth, and only half of the stator teeth are employed with PMs. The stator PMs and their adjacent stator teeth constitute the PM-iron structure. Compared with the aforementioned DSPM, SMTPM and SSPM, the STPM has lower PM usage and lower cost accordingly.

III. General Design Principle And Field Harmonic Analysis

A. General Design Principle

Although dual-PM excited machines have various types of configurations, the essential principle is that both the stator and the rotor should have PM-iron structure, which can provide both PM excitation and flux modulation. The working principle of the dual-PM machines is based on the flux modulating effect. The final harmonics, which refer to the field harmonics after modulated by the stator and rotor, have different PPN and rotating speeds from the original harmonics when flux modulating effect is not considered. Besides the fundamental component, various harmonics will be induced by the asymmetrical reluctance distribution, harmonics with the same PPN and rotating speeds can interact to generate electromagnetic torque. To reveal the working principle of the dual-PM excited machines, the magnetic fields excited by the two sets of PMs and armature currents should be studied. The magnetic field excited by the stator PMs will be modulated by the rotor, the PPN and rotating speeds of the final harmonics excited by the stator PMs can be expressed as

$$\begin{cases} p_s^f(m,i) = \left|mp_s + iN_r\right| \\ \Omega_s^f(m,i) = \dfrac{iN_r}{mp_s + iN_r}\Omega_r \\ m = 1,2,3... \\ i = 0,\pm1,\pm2... \end{cases} \tag{1}$$

where the superscript f refers to the final harmonics, p_s is the original PPN of the stator PMs, N_r is the number of modulator on the rotor, and Ω_r refers to the rotor speed in the reference of stator. We can find that although the stator PMs are stationary located on the stator, some rotating harmonics can be generated due to the modulating effect of the rotor.

The magnetic field excited by the rotor PMs can be analyzed in a similar way. The PPN and rotating speeds of the final harmonics excited by the rotor PMs can be expressed as

$$\begin{cases} p_r^f(n,j) = \left|np_r + jN_s\right| \\ \Omega_r^f(n,j) = \dfrac{np_r}{np_r + jN_s}\Omega_r \\ n = 1,2,3... \\ j = 0,\pm1,\pm2... \end{cases} \tag{2}$$

where p_r is the original PPN of the rotor PMs, N_s is the number of modulator on the stator. To generate steady electromagnetic torque, the magnetic fields excited by both the stator PMs and the rotor PMs should interact with the armature field. The PPN and rotating speeds of the magnetic field excited by the stator PMs and rotor PMs should be equal to that excited by armature currents, which means

$$\begin{cases} p_a = \left|mp_s + iN_r\right|; \quad \Omega_a = \dfrac{iN_r}{mp_s + iN_r}\Omega_r \\ p_a = \left|np_r + jN_s\right|; \quad \Omega_a = \dfrac{np_r}{np_r + jN_s}\Omega_r \end{cases} \tag{3}$$

As the low-order harmonics are prominent in generating electromagnetic torque, only $m=1$, $n=1$, $j=\pm1$ and $i=\pm1$ are considered. One can find that with $j=1, i=-1$ and $j=-1, i=1$, the equations cannot be solved. The PPN of the stator PMs and the rotor PMs, the number of the flux modulator on the stator and the rotor, the PPN and rotating speed of the armature field should satisfy

$$\begin{cases} N_r = p_r \\ N_s = p_s \\ p_a = p_s + p_r \\ \Omega_a = \dfrac{p_r}{p_s + p_r}\Omega_r \end{cases} \tag{4}$$

when $j=1, i=1$, and

$$\begin{cases} N_r = p_r \\ N_s = p_s \\ p_a = \left|p_r - p_s\right| \\ \Omega_a = \dfrac{p_r}{p_r - p_s}\Omega_r \end{cases} \tag{5}$$

when $j=-1, i=-1$.

From Eq. (4) and Eq. (5), the general design principle of the dual-PM machines can be deduced, in which the PPN of the stator PMs should equal to the number of modulators on the stator, and the PPN of the rotor PMs should also equal to the number of modulators on the rotor. This is the reason why PM-iron sequence should be employed on both the stator and the rotor in dual-PM machines, because the PPN of PMs and the number of modulators in the PM-iron sequence are the same. The PPN and rotating speed of the armature field are governed in a similar way as magnetic gear.

TABLE I.
EFFECTIVE FIELD HARMONICS WHEN $p_a = p_s + p_r$

Effective Harmonic Pairs [$H_s^f(m,i)$, $H_r^f(n,j)$, $H_a^f(k,t)$]	Pole-Pair Number(PPN)	Rotational Speed
[$H_s^f(1,0)$, $H_a^f(-1,0)$]	$p_s = \left\|p_a - p_r\right\|$	$0 = [p_a\Omega_a - p_r\Omega_r]/[p_a - p_r]$
[$H_s^f(1,1)$, $H_r^f(1,1)$, $H_a^f(0,0)$]	$p_s + p_r = p_a$	$p_r\Omega_r/[p_s + p_r] = \Omega_a$
[$H_s^f(1,-1)$, $H_r^f(1,-1)$]	$\left\|p_r - p_s\right\|$	$p_r\Omega_r/[p_r - p_s]$
[$H_s^f(1,2)$, $H_a^f(1,0)$]	$p_s + 2p_r = p_a + p_r$	$2p_r\Omega_r/[p_s + 2p_r] = [p_a\Omega_a + p_r\Omega_r]/[p_a + p_r]$
[$H_r^f(1,0)$, $H_a^f(0,-1)$]	$p_r = \left\|p_a - p_s\right\|$	$\Omega_r = p_a\Omega_a/[p_a - p_s]$
[$H_r^f(1,2)$, $H_a^f(0,1)$]	$p_r + 2p_s = p_a + p_s$	$p_r\Omega_r/[p_r + 2p_s] = p_a\Omega_a/[p_a + p_s]$

TABLE II.
EFFECTIVE FIELD HARMONICS WHEN $p_a = p_r - p_s$, $p_r > p_s$

Effective Harmonic Pairs [$H_s^f(m,i)$, $H_r^f(n,j)$, $H_a^f(k,t)$]	Pole-Pair Number(PPN)	Rotational Speed
[$H_s^f(1,0)$, $H_a^f(-1,0)$]	$p_s = \left\|p_a - p_r\right\|$	$0 = [p_a\Omega_a - p_r\Omega_r]/[p_a - p_r]$
[$H_s^f(1,1)$, $H_r^f(1,1)$]	$p_s + p_r$	$p_r\Omega_r/[p_s + p_r]$
[$H_s^f(1,-1)$, $H_r^f(1,-1)$, $H_a^f(0,0)$]	$\left\|p_r - p_s\right\| = p_a$	$p_r\Omega_r/[p_r - p_s] = \Omega_a$
[$H_s^f(1,-2)$, $H_a^f(1,0)$]	$\left\|p_s - 2p_r\right\| = \left\|p_a + p_r\right\|$	$2p_r\Omega_r/[2p_r - p_s] = [p_a\Omega_a + p_r\Omega_r]/[p_a + p_r]$

[$H_r^f(1,0)$, $H_a^f(0,1)$]	$p_r = \lvert p_a + p_s \rvert$	$\Omega_r = p_a\Omega_a / [p_a + p_s]$
[$H_r^f(1,-2)$, $H_a^f(0,-1)$]	$\lvert p_r - 2p_s \rvert = \lvert p_a - p_s \rvert$	$p_r\Omega_r / [p_r - 2p_s] = p_a\Omega_a / [p_a - p_s]$

TABLE III.
EFFECTIVE FIELD HARMONICS WHEN $p_a = p_s - p_r$, $p_r < p_s$

Effective Harmonic Pairs [$H_s^f(m,i)$, $H_r^f(n,j)$, $H_a^f(k,t)$]	Pole-Pair Number(PPN)	Rotational Speed
[$H_s^f(1,0)$, $H_a^f(1,0)$]	$p_s = \lvert p_a + p_r \rvert$	$0 = [p_a\Omega_a + p_r\Omega_r] / [p_a + p_r]$
[$H_s^f(1,1)$, $H_r^f(1,1)$]	$p_s + p_r$	$p_r\Omega_r / [p_s + p_r]$
[$H_s^f(1,-1)$, $H_r^f(1,-1)$, $H_a^f(0,0)$]	$\lvert p_r - p_s \rvert = p_a$	$p_r\Omega_r / [p_r - p_s] = \Omega_a$
[$H_s^f(1,-2)$, $H_a^f(1,0)$]	$\lvert p_s - 2p_r \rvert = \lvert p_a - p_r \rvert$	$2p_r\Omega_r / [2p_r - p_s] = [p_a\Omega_a - p_r\Omega_r] / [p_a - p_r]$
[$H_r^f(1,0)$, $H_a^f(0,-1)$]	$p_r = \lvert p_a - p_s \rvert$	$\Omega_r = p_a\Omega_a / [p_a - p_s]$
[$H_r^f(1,-2)$, $H_a^f(0,1)$]	$\lvert p_r - 2p_s \rvert = \lvert p_a + p_s \rvert$	$p_r\Omega_r / [p_r - 2p_s] = p_a\Omega_a / [p_a + p_s]$

B. Field Harmonic Analysis

As mentioned in Eq. (4) and Eq. (5), there are two kinds of methods to determine the pole-pair combination of dual-PM machines. The PPN of the armature field can be either the sum of the PPN of rotor PMs and the PPN of stator PMs, or the absolute value of the minus of the PPN of rotor PMs and the PPN of stator PMs. It should be noted that the fundamental component of armature field will also be modulated by both the stator and the rotor. The PPN and rotating speeds of the final harmonics excited by the armature currents can be expressed as

$$\begin{cases} p_a^f(k,t) = \lvert p_a + kN_r + tN_s \rvert \\ \Omega_a^f(k,t) = \dfrac{p_a\Omega_a + kN_r\Omega_r}{p_a + kN_r + tN_s} \end{cases} \quad (6)$$

where k and t are all integers. When the pole-pair combination is determined according to Eq. (4), those effective field harmonics which are capable of generating stable electromagnetic torques are listed in Table I. When the pole-pair combination is determined according to Eq. (5), the PPN of the armature field p_a is equal to $p_r - p_s$ when $p_r > p_s$, and equal to $p_s - p_r$ when $p_r < p_s$, those main effective field harmonics in the air-gap are listed in Table II and Table III, respectively.

From Table I to Table III, we can find that besides the fundamental field components excited by the stator PMs, rotor PMs and armature currents, most of the low-order harmonics introduced by the flux modulating effect are also synchronous and can contribute to the effective electromagnetic torque generation. Therefore, the torque capability of the dual-PM machines can be improved.

IV. DESIGN OPTIMIZATION AND COMPARISON

A. Design Optimization

The electromagnetic performances of these four types of dual-PM machines are analyzed and compared. Before comparison, all the four dual-PM machines are optimized using ITS-FEM coupled method. The flowchart of the ITS-FEM coupled method is shown in Fig. 3. Firstly, an initial solution is randomly generated. Starting from a current solution x, a series of neighborhood solutions x_1, x_2,..., x_p will be generated around x by the algorithm, and the best solution x^* will be chosen from these neighborhood solutions. This best solution x^* is labeled as the new current solution and

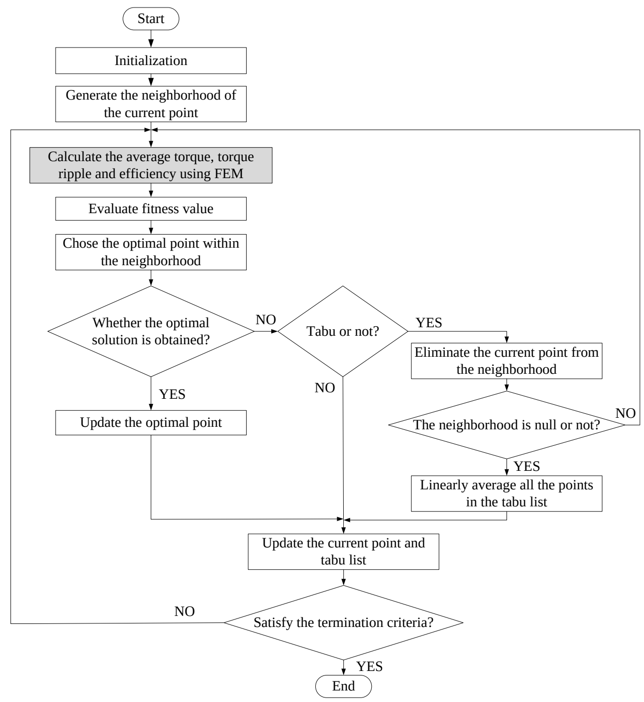

Fig. 3. Flowchart of the ITS-FEM coupled method.

begin a new cycle of iterations. This optimization process will continue until a stop criterion is satisfied. In traditional stochastic optimization algorithms, the current solution x changes into the next solution x^* if the value of the objective function is getting better. In this case, the optimization tends to get trapped easily to the local best solution rather than the global best. In this paper, the used ITS algorithm chooses the local best solution instead of the global best solution as the new current one, so as to avoid falling into a local best solution. Moreover, an adaptive step vector is used in the implementation of moves. All the variables are normalized and a standard step vector h with a controlled step-size is set in different directions

$$h_i = h_{i-1} / c_k (c_k = L^{\frac{1}{n-1}}, h_1 = 1), \quad i = 1, 2, ..., n \quad (7)$$

where L refers to the user-defined step size level, which stipulates a minimal step-size $1/L$ in h. And the update principle is given as

$$x_j^* = x_j + r p_j h_i \tag{8}$$

where r is randomly generated within [-1,1], p_j is the coefficient vector p in the j th direction and can be expressed as

$$p_j = \left(b_j - a_j\right)/2, \qquad j = 1, 2, ..., n \tag{9}$$

where b_j and a_j refer to the range of p_j. It should be noted that $h_1 = 1$ is always defined to guarantee the global searching ability. The adaptively controlled step size can effectively improve the searching efficiency and accelerate the convergence.

Three objectives are investigated, which include the average output torque f_1, the torque ripple ratio f_2 and the efficiency f_3. The optimal design problem is formulated as

$$\min\left\{-f_1(x), f_2(x), -f_3(x)\right\}, \qquad x \in F \tag{10}$$

where x refers to the design parameters and listed in Table IV, F refers to the constraints of the design parameters, and f_2 can be expressed in Eq. (11), where $T_{\max}$ and $T_{\min}$ are the maximum value and minimum value of the steady torque, respectively.

$$f_2(x) = \frac{T_{\max} - T_{\min}}{f_1(x)} \tag{11}$$

TABLE IV.
PARAMETERS NEED TO BE OPTIMIZED AND THEIR LIMITS

Parameters	DSPM		SMTPM		SSPM		STPM	
	Upper value	Lower value	Upper value	Lower value	Upper value	Lower value	Upper value	Lower value
Gap-side stator diameter(mm)	67	60	65	58	66	53	65	51
Rotor PM thickness(mm)	5	2	5.5	2	5.5	2	5.5	1.5
Rotor PM ratio	80%	30%	80%	30%	80%	30%	80%	30%
Stator PM thickness(mm)	5	2	5.5	2	2.5	1	5.5	1.5
Stator PM ratio	80%	30%	80%	30%	-	-	-	-
Stator tooth width(mm)	-	-	-	-	9	5	9	5

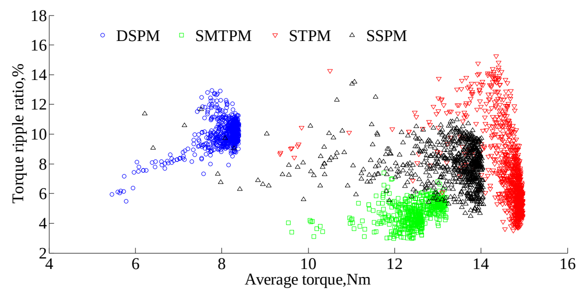

Fig. 4. The relationship between the torque ripple ratio and average torque.

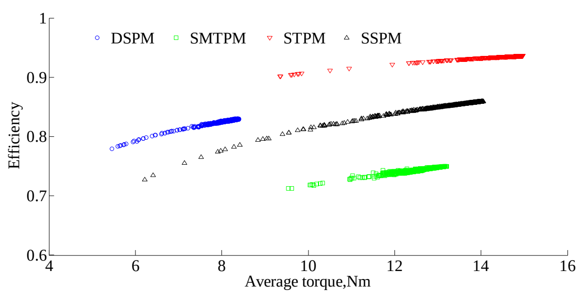

Fig. 5. The relationship between the efficiency and average torque.

The parameterized FE model of these four machines are built using Maxwell package. In this paper, only structural parameters are optimized. The overall diameter and axial length are fixed at 90 mm and 80 mm, respectively. The parameters that need to be optimized and their limits are listed in Table IV. The stator PM ratio and rotor PM ratio are defined as the ratio of the PM arc to the total pole arc. Fig. 4 shows the optimization results of the torque ripple ratio and the average output torque, and the relationship between the efficiency and the average output torque is given in Fig. 5. It can be observed that the efficiency is positive correlated with the average output torque, when the output torque increases, the efficiency of all the four dual-PM machines increases accordingly. Therefore, the efficiency and the average output torque can be combined into one single objective during optimization, when the maximum average torque is obtained, the maximum efficiency is achieved as well.

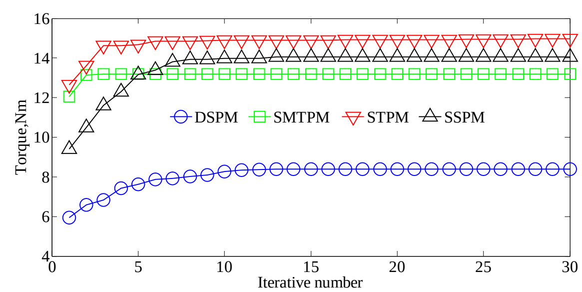

Fig. 6. Optimal average torque at different iterative number.

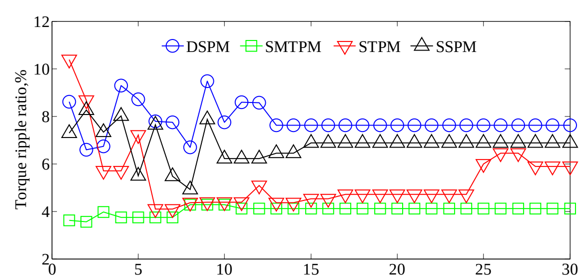

Fig. 7. Torque ripple ratio at different iterative number.

After the aforementioned multi-objective optimization, all the four dual-PM machines studied in this paper are optimized through single objective optimization. The objective is to achieve the optimal output torque when excited with a fixed current density 8 A/mm^2, the constraint is all the machines should have a torque ripple ratio lower than 12%. The average output torque versus iterative number is shown in Fig. 6. One can find that SMTPM, SSPM and STPM can achieve larger output torque than DSPM, and the optimization can converge within around 10 iterations, which shows the effectiveness of the optimization method. The corresponding torque ripple ratio is given in Fig. 7, one can find that all the torque ripple ratios are lower than 12%, which consists with the constraint of single objective optimization. According to the optimization results, SMTPM has smaller torque ripple ratio. From Fig. 5 and Fig. 6, one can see that although the SMTPM can achieve large output torque, its efficiency is very low. The reason behind this is that the SMTPM has significant short-circuit leakage flux, which will greatly increase the iron loss and eddy current loss, and reduce the efficiency consequently. The final design parameters after optimization are given in Table V.

TABLE V
FINAL DESIGN PARAMETERS

Parameters	DSPM	SMTPM	SSPM	STPM
Total diameter(mm)	90			
Gap-side stator diameter(mm)	64	61.7	64.2	62.6
Air-gap length(mm)	0.5			
Rotor PM thickness(mm)	4.5	4.9	4.6	4.3
Rotor PM ratio	50%			
Stator PM thickness(mm)	4	2.5	2.5	5.5
Stator PM ratio	55%	50%	-	-
Stator tooth width(mm)	-	-	5	6.4
Stack length(mm)	80			
PPN of stator PM	14	36	12	6
PPN of rotor PM	19	41	17	11
PPN of armature field	5			
Number of stator slots	12			
Number of phases	3			
Turns of conductors	60	50	50	65
Remanence of NdFeB(T)	1.1			
Relative permeability of NdFeB	1.05			

B. *Comparative Study*

The electromagnetic performances of the proposed four types of dual-PM machines are studied and compared using FEM. Firstly, in order to verify the analytical investigation given in section III, the air-gap flux density excited by the stator PMs, rotor PMs and armature currents are calculated, as shown in Fig. 8. Frozen permeability method [25] is used when calculating the magnetic fields, so as to investigate the magnetic field excited by the stator PMs, rotor PMs and armature currents separately. The field harmonic components are shown in Fig. 9, one can find that besides the original field harmonics excited by the PMs and armature currents, many other harmonics are generated due to the bidirectional flux modulating effect enabled by the uneven permeance distribution of the stator and rotor, and most of the predominant harmonics with high amplitudes have the same pole-pairs and are working harmonics. The results from FEM show good agreement with the analytical results listed in Table II.

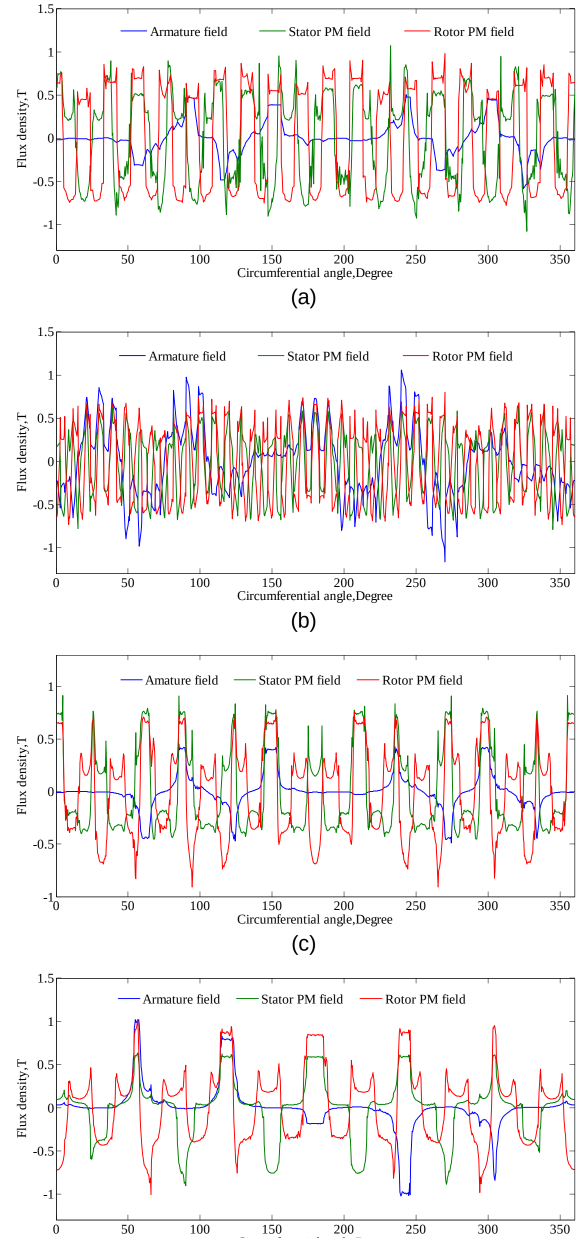

Fig. 8. Air-gap field distributions. (a) DSPM. (b) SMTPM. (c) SSPM. (d) STPM.

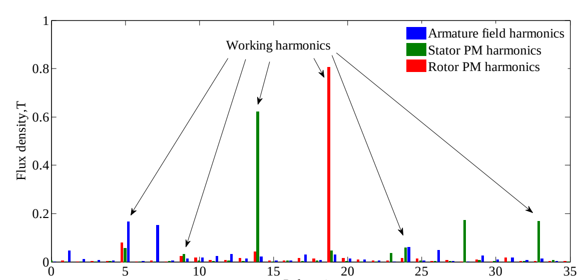

(a)

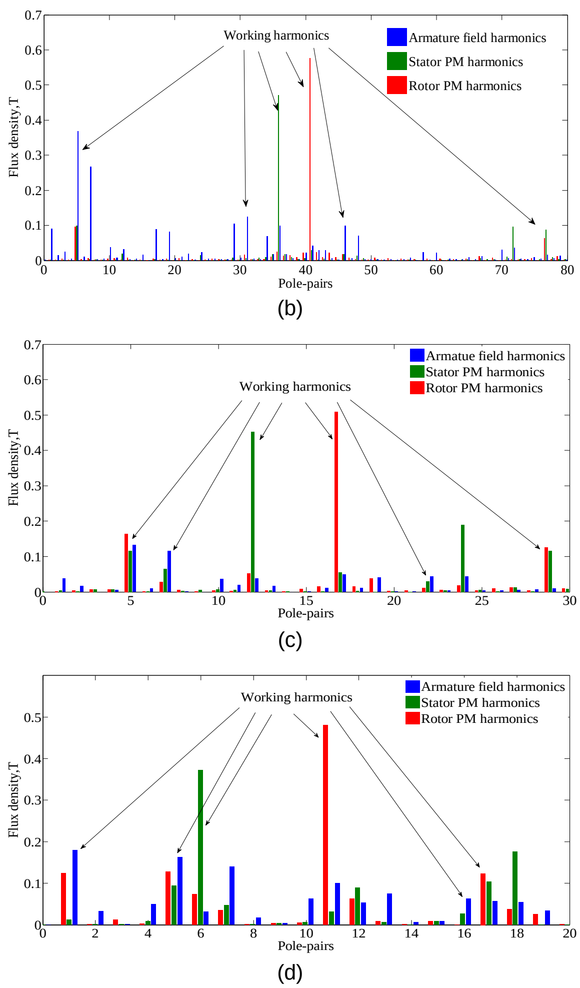

Fig. 9. Air-gap field harmonics. (a) DSPM. (b) SMTPM. (c) SSPM. (d) STPM.

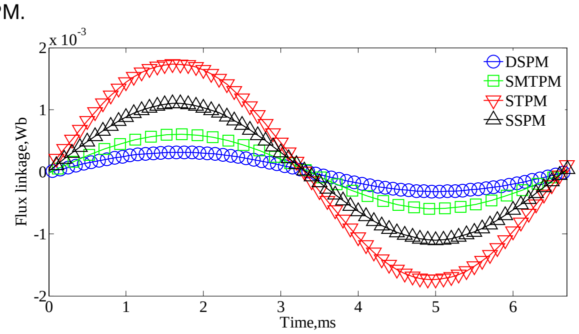

Fig. 10. Flux linkage waveforms of the single turn conductor.

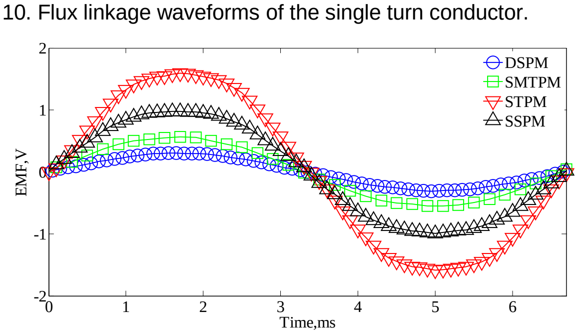

Fig. 11. No load back EMF waveforms of the single turn conductor.

Fig. 10 shows the flux linkage of the single turn conductor, and the rotating speeds are 474 rpm for DSPM, 220 rpm for SMTPM, 529 rpm for SSPM and 818 rpm for STPM, therefore the frequency of the flux linkage for all the four machines is the same, which is 150Hz. One can find that the STPM has the highest flux linkage per single turn conductor, similar phenomenon can be observed in the EMF waveforms shown in Fig. 11. This means that the STPM has the lowest flux leakage, and can achieve high output torque and high efficiency as shown in Fig. 5 and Fig. 6.

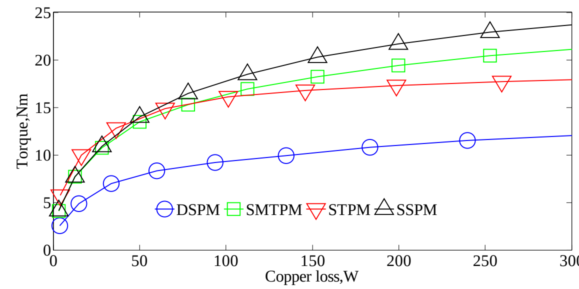

Fig.12. Output torque at different copper loss.

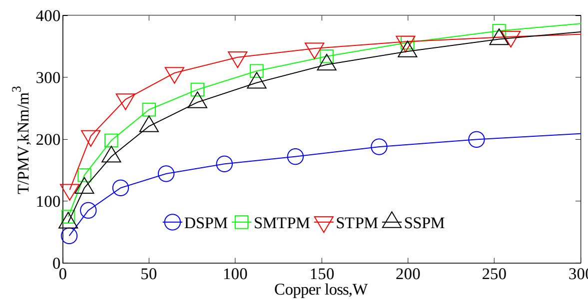

Fig. 13. T/PMV at different copper loss.

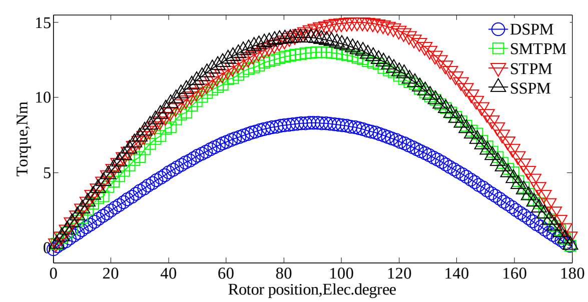

Fig. 14. Torque-angle waveforms.

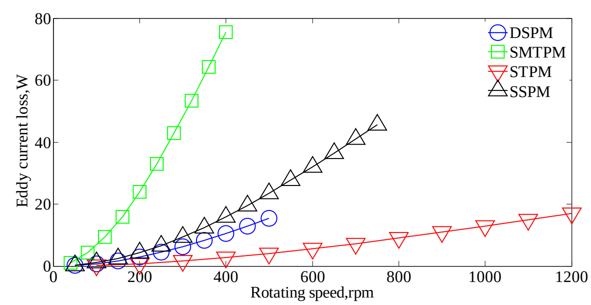

Fig. 15. Eddy current loss at different speeds.

Fig. 12 shows the output torque of the investigated dual-PM machines at different copper loss. One can find that the output torque increases with the increasing of copper loss, because the increasing of copper loss means the armature current is increased. However, the increasing speed becomes slower and the curves become flat when the copper loss is large, and the reason behind this is the magnetic saturation when the copper loss is high. Compared with the other three machines, the

STPM is more likely to suffer magnetic saturation, which reduces its torque capability when large armature current is applied and the copper loss is high. Therefore, STPM is more suitable for low armature current applications. Since the output torque of PM machine is greatly influenced by the PM consumption, the torque per PM volume (T/PMV) is investigated, as shown in Fig. 13. One can see that the STPM machine has the highest T/PMV when low current density is applied and the copper loss is small. SMTPM and SSPM also have large T/PMV compared with DSPM. Due to magnetic saturation, the T/PMV of STPM has little increase when the copper loss is high. The stationary torque waveforms when the applied current density is 8 A/mm^2 are calculated and given in Fig. 14. From the aforementioned comparative studies, we can find that among the four typical dual-PM machines investigated in this paper, the STPM has the best overall electromagnetic performances, which include high output torque, low torque ripple ratio, high efficiency and high T/PMV. The eddy current losses of the four machines are studied and compared, as given in Fig. 15. One can find that the eddy current loss increases with the increasing of rotating speeds. Since the four machines have different rotor pole-pairs, the speed range is different accordingly. Among all the four machines studied, SMTPM has the largest eddy current loss due to its high leakage flux and results in low efficiency. The eddy current loss of STPM is the smallest, which contributes to achieve high torque density and high efficiency. The detailed comparison of electromagnetic performances are given in Table VI.

TABLE VI
ELECTROMAGNETIC PERFORMANCES COMPARISON

Items	DSPM	SMTPM	SSPM	STPM
Rated power (W)	412	313	776	1276
Rated speed (rpm)	474	220	529	818
Rated torque (Nm)	8.3	13.5	14	14.9
Power factor	0.78	0.63	0.73	0.91
PM usage(cm^3)	57.6	54.5	63.5	48.5
Rated T/PMV(kNm/m^3)	144	248	220	307

V. EXPERIMENTAL VERIFICATION

To verify the proposed design of the dual-PM machines, a prototype of the STPM is manufactured, according to the parameters shown in Table V. The assembled stator and rotor, and experimental platform are shown in Fig. 16. A servo motor is used to provide the load torque, and the tested waveforms can be displayed on the oscilloscope.

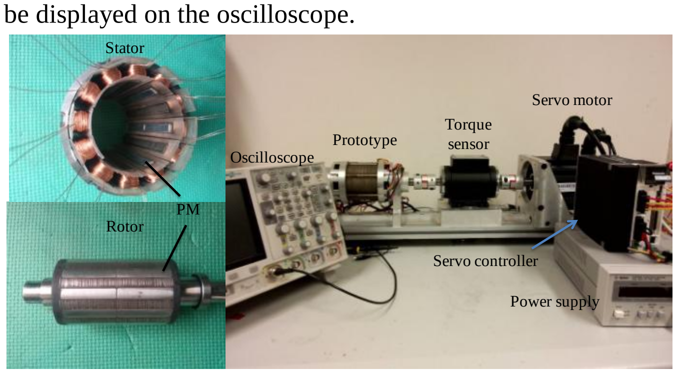

Fig. 16. Experimental platform.

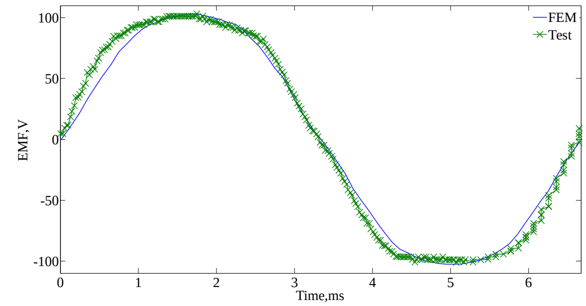

Fig. 17. No load back EMF waveforms.

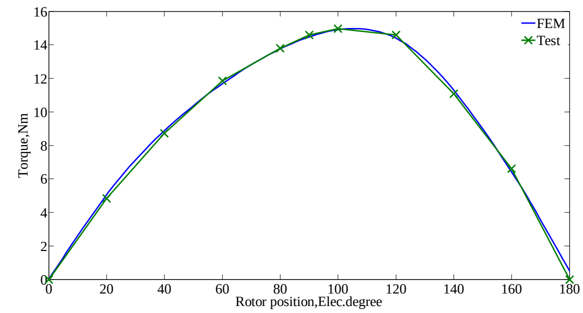

Fig. 18. Stationary torque waveforms.

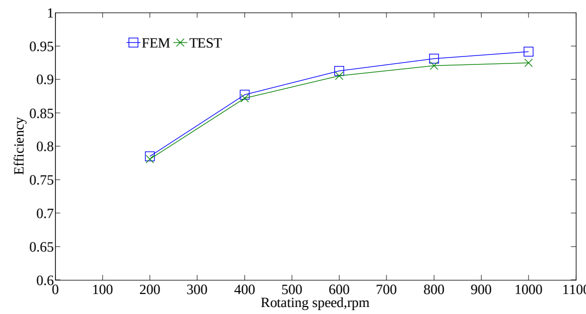

Fig. 19. Efficiency of STPM at different speeds.

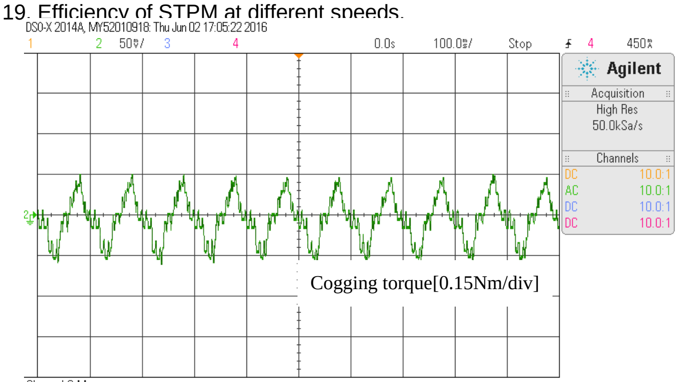

Fig. 20. Cogging torque waveform.

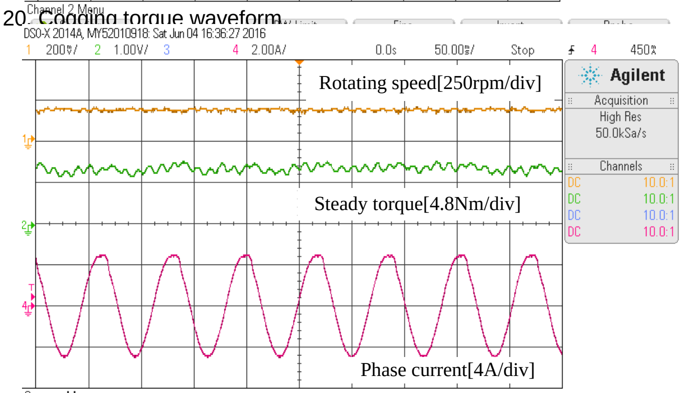

Fig. 21. Waveforms of steady torque, rotating speed and phase current.

Firstly, the no load back EMF when the machine runs at 818 rpm is tested and compared with the result of FEM, as shown in Fig. 17. One can find good agreement between the waveforms of experimental test and FEM. Since the prototype is made without additional cooling facilities, only small currents are applied during experiments for safety reasons. The stationary torque when the current density is 8 A/mm^2 are tested and compared with the FEM results, as shown in Fig. 18. Again, good agreement can be observed. Keeping the current density unchanged, the efficiency of STPM is tested when the machine runs at different speeds, and compared with the FEM results, as shown in Fig. 19. It can be observed that the proposed STPM can achieve high efficiency operation over a wide speed range. The tested efficiency is relatively lower than the simulated one, which is because mechanical loss is not considered during simulation. Fig. 20 shows the tested cogging torque waveform, the peak-peak value of the cogging torque is 0.3 Nm, which is an acceptable value. Finally, the steady torque when the machine runs at 200 rpm and the RMS current is 3.6 A is tested, the torque waveform and rotating speed as well as phase current waveform are all displayed on the oscilloscope, as shown in Fig. 21. We can see that steady electromagnetic torque can be generated by the manufactured STPM. The experimental tests can well verify the electromagnetic design.

VI. CONCLUSION

This paper systematically studies a new kind of machines with both stator and rotor PM excitations, namely, dual-PM excited machines. The PM-iron structure employed on both the stator and the rotor is the basis of the dual-PM machines, which can provide PM excitation and flux modulation simultaneously. The general design principle of the dual-PM machine is derived, and the air-gap field harmonics are investigated analytically. Four typical machine configurations are investigated and compared, in which STPM is firstly proposed in this paper. All the machines are optimized using ITS-FEM coupled method, their electromagnetic performances are comprehensively studied and compared. A STPM is manufactured and the experimental results well verify its electromagnetic design. Compared with other three machines, the proposed STPM can achieve the best overall performances due to its lowest leakage flux. The PM flux in STPM can effectively link the coil and contribute to the electromagnetic torque generation. Meanwhile, iron loss and eddy current loss can be reduced when the leakage flux is reduced, which can result in high efficiency.

References

[1] K. T. Chau, C. C. Chan, and C. Liu, "Overview of permanent-magnet brushless drives for electric and hybrid electric vehicles," *IEEE Trans. Ind. Electron.*, vol. 55, pp. 2246-2257, Jun 2008.

[2] Y. Amara, L. Vido, M. Gabsi, E. Hoang, A. H. Ben Ahmed, and M. Lecrivain, "Hybrid Excitation Synchronous Machines: Energy-Efficient Solution for Vehicles Propulsion," *IEEE Trans. Veh. Technol.*, vol. 58, pp. 2137-2149, Jun 2009.

[3] Q. Wang, S. Niu, S. Ho, W. Fu, and S. Zuo, "Design and analysis of novel magnetic flux-modulated mnemonic machines," *IET Electric Power Applications*, vol. 9, pp. 469-477, 2015.

[4] Q. Wang and S. Niu, "Overview of flux-controllable machines: Electrically excited machines, hybrid excited machines and memory machines," *Renewable and Sustainable Energy Reviews*, vol. 68, pp. 475-491, 2017.

[5] Y. Fan, K. T. Chau, and S. Niu, "Development of a New Brushless Doubly Fed Doubly Salient Machine for Wind Power Generation," *IEEE Trans.Magn.*, vol. 42, pp. 3455-3457, 2006.

[6] R. Datta and V. T. Ranganathan, "Variable-speed wind power generation using doubly fed wound rotor induction machine - A comparison with alternative schemes," *IEEE Trans. Energy Convers.*, vol. 17, pp. 414-421, Sep 2002.

[7] Y. Liu, S. Niu, and W. Fu, "Design of an Electrical Continuously Variable Transmission Based Wind Energy Conversion System," *IEEE Trans. Ind. Electron.*, vol. 63, pp. 6745-6755, 2016.

[8] J. Hong, S. Park, D. Hyun, T.-j. Kang, S. B. Lee, C. Kral, *et al.*, "Detection and classification of rotor demagnetization and eccentricity faults for PM synchronous motors," *IEEE Trans. Ind. Appl.*, vol. 48, pp. 923-932, 2012.

[9] F. Zhou, J. Shen, W. Fei, and R. Lin, "Study of retaining sleeve and conductive shield and their influence on rotor loss in high-speed PM BLDC motors," *IEEE Trans.Magn.*, vol. 42, pp. 3398-3400, 2006.

[10] L. Wu, R. Qu, and D. Li, "Reduction of Rotor Eddy-Current Losses for Surface PM Machines With Fractional Slot Concentrated Windings and Retaining Sleeve," *IEEE Trans.Magn.*, vol. 50, pp. 1-4, 2014.

[11] T. H. Kim and J. Lee, "A study of the design for the flux reversal machine," *IEEE Trans.Magn.*, vol. 40, pp. 2053-2055, 2004.

[12] W. Zhao, J. Ji, G. Liu, Y. Du, and M. Cheng, "Design and analysis of a new modular linear flux-reversal permanent-magnet motor," *IEEE Trans. Appl. Supercond.*, vol. 24, pp. 1-5, 2014.

[13] D. S. More and B. G. Fernandes, "Modelling and performance of three-phase 6/14 pole flux reversal machine," *IET Electric Power Applications*, vol. 7, pp. 131-139, 2013.

[14] K. T. Chau, J. Z. Jiang, and W. Yong, "A novel stator doubly fed doubly salient permanent magnet brushless machine," *IEEE Trans.Magn.*, vol. 39, pp. 3001-3003, 2003.

[15] X. Zhu, M. Cheng, W. Hua, J. Zhang, and W. Zhao, "Design and Analysis of a New Hybrid Excited Doubly Salient Machine Capable of Field Control," in *Industry Applications Conference, 2006. 41st IAS Annual Meeting. Conference Record of the 2006 IEEE*, 2006, pp. 2382-2389.

[16] X. Zhu, L. Wang, Y. Chen, L. Chen, and L. Quan, "A Non-Rare-Earth Doubly Salient Flux Controllable Motor Capable of Fault-Tolerant Control," *IEEE Trans.Magn.*, vol. 51, pp. 1-4, 2015.

[17] W. Yu and D. Zhiquan, "Comparison of Hybrid Excitation Topologies for Flux-Switching Machines," *IEEE Trans.Magn.*, vol. 48, pp. 2518-2527, 2012.

[18] R. P. Deodhar, A. Pride, S. Iwasaki, and J. J. Bremner, "Performance Improvement in Flux-Switching PM Machines Using Flux Diverters," *IEEE Trans. Ind. Appl.*, vol. 50, pp. 973-978, 2014.

[19] H. Yang, H. Lin, Z. Q. Zhu, D. Wang, S. Fang, and Y. Huang, "A Variable-Flux Hybrid-PM Switched-Flux Memory Machine for EV/HEV Applications," *IEEE Trans. Ind. Appl.*, vol. 52, pp. 2203-2214, 2016.

[20] S. L. Ho, Y. Shiyou, N. Guangzheng, and H. C. Wong, "An improved Tabu search for the global optimizations of electromagnetic devices," *IEEE Trans.Magn.*, vol. 37, pp. 3570-3574, 2001.

[21] S. Peng, W. Fu, and S. Ho, "A Novel High Torque-Density Triple-Permanent-Magnet-Excited Magnetic Gear," *IEEE Trans.Magn.*, vol. 50, pp. 1-4, 2014.

[22] J. Shi and Z. Zhu, "Analysis of Novel Multi-Tooth Variable Flux Reluctance Machines With Different Stator and Rotor Pole Combinations," *IEEE Trans.Magn.*, vol. 51, pp. 1-11, 2015.

[23] C. Liu, K. T. Chau, and J. Z. Jiang, "A permanent-magnet hybrid brushless integrated starter-generator for hybrid electric vehicles," *IEEE Trans. Ind. Electron.*, vol. 57, pp. 4055-4064, 2010.

[24] I. A. A. Afinowi, Z. Q. Zhu, Y. Guan, J. C. Mipo, and P. Farah, "Hybrid-Excited Doubly Salient Synchronous Machine With Permanent Magnets Between Adjacent Salient Stator Poles," *IEEE Trans.Magn.*, vol. 51, pp. 1-9, 2015.

[25] W. Chu and Z. Zhu, "Average torque separation in permanent magnet synchronous machines using frozen permeability," *IEEE Trans.Magn.*, vol. 49, pp. 1202-1210, 2013.

Qingsong Wang received the B.Sc. degree from the College of Automotive Engineering, Jilin University, Changchun, China, in 2012, and M.Sc. degree in the School of Automotive Studies, Tongji University, Shanghai, China, in 2015. He is currently pursuing a Ph.D. degree in the Department of Electrical Engineering at The Hong Kong Polytechnic University, Kowloon, Hong Kong.

His research interests include the design of novel electric machines, EV/HEV propulsion, and renewable energy systems.

Shuangxia Niu received the B.Sc. and M.Sc. degrees in electrical engineering from the School of Electrical Engineering and Automation, Tianjin University, Tianjin, China, in 2002 and 2005, respectively, and the Ph.D. degree in electrical engineering from the Department of Electrical and Electronic Engineering, The University of Hong Kong, Hong Kong, in 2009. Since 2009, she has been with The Hong Kong Polytechnic University, Kowloon, Hong Kong, where she is currently an Assistant Professor in the Department of Electrical Engineering. She has authored or coauthored over 60 papers in leading journals. Her research interests include the design and control of novel electrical machines and drives, renewable energy conversion systems, and applied electromagnetics.

Lin Yang received the B.Sc. degree from XIDIAN University, Xi'an, China, in 2008, the M.Sc degree from the department of Electrical engineering, Zhejiang University, Hangzhou, China, in 2011, and the Ph.D. degree from the Department of Electrical engineering, The Hong Kong Polytechnic University, Hong Kong, in 2015. He is currently an engineer in State Power Economic Research Institute, Beijing, China. His research interests include the design and control of electrical machines, renewable energy systems and power system modelling and analysis.